HEPATOLOGY

HEPATOLOGY, VOL. 63, NO. 3, 2016

Cholestasis-Induced Adaptive Remodeling of Interlobular Bile Ducts

Nachiket Vartak,[1*] Amruta Damle-Vartak,[1*] Beate Richter,[2] Olaf Dirsch,[2] Uta Dahmen,[2] Seddik Hammad,[1,3] and Jan G. Hengstler[1]

Cholestasis is a common complication in liver diseases that triggers a proliferative response of the biliary tree. Bile duct ligation (BDL) is a frequently used model of cholestasis in rodents. To determine which changes occur in the three-dimensional (3D) architecture of the interlobular bile duct during cholestasis, we used 3D confocal imaging, surface reconstructions, and automated image quantification covering a period up to 28 days after BDL. We show a highly reproducible sequence of interlobular duct remodeling, where cholangiocyte proliferation initially causes corrugation of the luminal duct surface, leading to an approximately five-fold increase in surface area. This is analogous to the function of villi in the intestine or sulci in the brain, where an expansion of area is achieved within a restricted volume. The increase in surface area is further enhanced by duct branching, branch elongation, and loop formation through self-joining, whereby an initially relatively sparse mesh surrounding the portal vein becomes five-fold denser through elongation, corrugation, and ramification. The number of connections between the bile duct and the lobular bile canalicular network by the canals of Hering decreases proportionally to the increase in bile duct length, suggesting that no novel connections are established. The diameter of the interlobular bile duct remains constant after BDL, a response that is qualitatively distinct from that of large bile ducts, which tend to enlarge their diameters. Therefore, volume enhancement is only due to net elongation of the ducts. Because curvature and tortuosity of the bile duct are unaltered, this enlargement of the biliary tree is caused by branching and not by convolution. *Conclusion:* BDL causes adaptive remodeling that aims at optimizing the intraluminal surface area by way of corrugation and branching. (HEPATOLOGY 2016;63:951-964)

The biliary network of the liver plays an important role in the formation and secretion of bile as well as excretion of toxic substances through bile ducts. Cholangiocytes, the cells that form bile ducts, are responsible for the secretion, reabsorption, and regulation of bile constituents.[1] Upon various pathological conditions, complex "ductular reactions" are observed that involve the proliferation of cholangiocytes.[2,3] Ductular reactions are typically caused by hepatotoxic chemicals or cholangiopathies, such as primary biliary cirrhosis, which lead to cholestasis.[4] These reactions are accompanied by inflammation, and although they are necessary for functional recovery, they have several effects under chronic conditions that are deleterious to liver function.[5] The most frequently used animal model of cholestasis is bile duct ligation (BDL) in rodents,[6] because this technique induces morphological changes comparable to those seen in human biliary cirrhosis.[7] However, little is known about the three-dimensional (3D) architecture of ductular reactions after BDL and how it leads to beneficial or deleterious outcomes after liver injury. Studies of cholestasis using micro-computed tomography (micro-CT) have been confined to investigation of larger ducts

Abbreviations: 2D, two-dimensional; 3D, three-dimensional; BDL, bile duct ligation; BrdU, bromodeoxyuridine; IgG, immunoglobulin G; micro-CT, micro-computed tomography.

Received July 8, 2015; accepted November 25, 2015.

Additional Supporting Information may be found at onlinelibrary.wiley.com/doi/10.1002/hep.28373/suppinfo.

This study was supported by the Virtual Liver Network, its successor Liver Systems Medicine and Lebersimulator projects funded by the German Federal Ministry of Education and Research (BMBF).

**These authors contributed equally to the study.*

View this article online at wileyonlinelibrary.com.

DOI 10.1002/hep.28373

Potential conflict of interest: Nothing to report.

with more than 30 μm diameter due to the limited resolution of this technique. However, the interlobular bile ducts that drain the hepatic lobules are approximately 10 μm in diameter, and 3D analysis by micro-CT is not possible. Confocal 3D studies of intrahepatic bile ducts describing their *de novo* formation during embryonic development,[8] or their response to toxic challenge[3] have recently become available. However, these two studies represent the entire corpus of currently available information regarding the remodeling of the biliary tree in 3D; spatio-temporal responses after BDL-induced cholestasis have not yet been published.

It has been reported that bile duct ligation leads to enlargement of duct diameter.[9] Moreover, routine pathological two-dimensional (2D) examinations typically show increased numbers of bile ducts per periportal field in cholestatic livers. Currently, it remains unclear whether the increased number results from a single hypertrophic convoluted duct intersecting the 2D slice level several times or from increased numbers of ducts. In the present study, we investigated 3D architectural changes of interlobular bile ducts to gain deeper insight into ductular reaction mechanisms.

Materials and Methods

A detailed description of all materials and methods along with information on sample sizes is provided in the Supporting Information. The custom program code and sample-wise tabulated data are available at http://vartak.org/liver.

ANIMALS AND BILE DUCT LIGATION

Common bile duct ligation was performed on C57BL/6N mice. Blood and liver samples were harvested at 0.25, 1, 3, 5, 7, 14, and 28 days post-BDL. For proliferation analysis, bromodeoxyuridine (BrdU) was injected 1 hour before harvest.[10] All animals received humane care in compliance and according to the criteria defined by the European Convention for the Protection of Vertebrate Animals used for Experimental and other Scientific Purposes (ETS 123).

ARCHITECTURAL IMMUNOSTAINING AND IMMUNOHISTOCHEMISTRY

Liver tissue was fixed immediately in 4% paraformaldehyde to prepare 50- to 75-μm-thick vibratome slices. Liver architecture staining was performed using anti-KRT19 and anti-DPP4 immunoglobulin G (IgG) based on modifications of methods described by Hammad et al.[10] Additionally, liver tissue harvested after BrdU injection was fixed in 4% formalin and embedded in paraffin for microtome sectioning.

IMAGING AND IMAGE ANALYSIS

3D confocal immunofluorescence stacks of liver tissue sections were obtained on an Olympus FV1000 microscope equipped with an HCL Apochromat 60× oil immersion objective at a resolution of 0.207 × 0.207 × 0.540 μm per pixel. These 3D stacks were then used for surface reconstructions and 3D morphometric analyses. Surface reconstructions of the 3D stacks were generated using IMARIS (Bitplane AG). Measurement of duct diameter, eccentricity, tortuosity, volume, duct branching, biliary tree complexity, luminal surface area, luminal surface corrugation, distance from the associated portal vein, and frequency of Hering canals was performed using custom software developed by the authors. Additionally,

ARTICLE INFORMATION:

From the [1]Department of Systems Toxicology, Leibniz Institute for Work Physiology and Human Factors (IfADo) at TU Dortmund, Dortmund, Germany; the [2]Department of Experimental Transplantation Surgery, University Clinic Jena, Jena, Germany; and the [3]Faculty of Veterinary Medicine, South Valley University, Qena, Egypt.

ADDRESS CORRESPONDENCE AND REPRINT REQUESTS TO:

Nachiket Vartak, Ph.D.
Department of Systems Toxicology
Leibniz Institute for Work Physiology and Human Factors
(IfADo) at TU Dortmund
44139 Dortmund, Germany.
E-mail nash@ifado.de
or

Jan Hengstler, M.D.
Department of Systems Toxicology
Leibniz Institute for Work Physiology and Human Factors
(IfADo) at TU Dortmund
44139 Dortmund, Germany.
E-mail: hengstler@ifado.de
Fax: +49-231-1084-403

cholangiocyte proliferation rates were determined from automated analysis of brightfield slide scans of anti-BrdU-stained paraffin sections.

Results

BILE DUCT LIGATION RELIABLY INDUCES CHOLESTASIS

To confirm the efficacy of BDL to induce cholestasis and ductular reactions, liver tissue blocks were sectioned ~200 μm below the convex surface of the liver lobe to guarantee reproducible acquisition of the terminal branches and features of the biliary tree (Fig. 1A,B). Anti-BrdU staining of these liver slices from BrdU-treated mice showed an increase in BrdU-positive cells, reflecting the increased cellular proliferation rate of cholangiocytes in terminal bile ducts (Fig. 1C). Cellular proliferation rate peaked at day 3 post-BDL and decreased at later times until day 28 post-BDL. Analysis of serum samples from these mice showed elevated serum markers for acute liver injury at early time points, whereas serum bilirubin increased until day 14 post-BDL and plateaued at later times (Supporting Fig. S1) at elevated levels, indicating a jaundiced state. Together, these data confirm that BDL in mice induced cholestasis as intended and triggered the associated ductular reaction of increased proliferation.

We then performed immunofluorescence-based architectural staining of liver slices from BDL mice. Anti-DPP4 antibody marks the canaliculi between hepatocytes, the luminal surface of the bile duct, and the luminal surface of the sinusoidal networks. Anti-mouse IgG marks the lobular sinusoidal network and blood vessels, whereas anti-KRT19 IgG marks only cholangiocytes and thereby the biliary tree. Confocal 3D scans of these tissues were then converted to isosurface representations using manual 3D reconstruction (Fig. 1E; for 2D projections, see Supporting Fig. S2A). A combination of surface- and channel-based segmentation yields surface reconstructions of the entire stack of liver tissue. Reconstructions of periportal fields 3, 7, 14, and 28 days post-BDL revealed that all the relevant features, bile ducts, and their links to the canalicular network (canals of Hering) are well presented (Fig. 1F).

BILIARY TREE REMODELING BY ELONGATION, BRANCHING, AND LOOPING

Because the increase in cholangiocytes observed after BDL results in an increase in ductular tissue, we investigated its influence on bile duct morphology. Duct elongation and duct widening (diameter) are basic parameters that have been reported to undergo changes following injury to the biliary tree. Using segmented bile ducts from the surface reconstructions, we developed automatic analysis of bile duct length, diameter, and volume at various times post-BDL. Duct length increased in a biphasic manner between days 3 and 7 as well as between days 7 and 28 (Fig. 2). We further investigated the nature of this ductular elongation in terms of changes to its convolution (i.e., its "twistedness"). Duct convolution is a possible mechanism by which the additional length generated by the ductular reaction may be accommodated within the tissue. Convolution is an ill-defined parameter and is a function of at least two out of three interdependent variables: (1) the curvature of the duct along its length, (2) the ratio of the duct length to the straight-line distance between its endpoints, and (3) the frequency of inflection points along the length of the duct. We measured the curvature and tortuosity and determined that while bile ducts have some inherent twistedness, both these parameters do not change substantially over the 28 days following BDL (Fig. 2C,D). The lack of convolution in mouse bile ducts following BDL is congruous to similar observations in rats wherein ductular reactions were induced through α-naphthylisothiocyanate toxicity.[9]

An alternative mechanism by which the increased length may be accommodated is by branching of the bile duct. We found that the number of branches in bile ducts increases during the first 14 days following BDL (Fig. 2E). Fitting this branch frequency data to a logistic equation yielded a Hill coefficient of 3.73 with a maximal branch formation occurring at 6.7 days (R^2 = 0.99). The Hill coefficient value of >1 indicates a strong cooperative effect[11] in branch formation, showing that existing branches tend to produce more branches. Curiously, the branch frequency did not increase further between days 14 and 28 even though significant cell proliferation (see Fig. 1D) and duct elongation (see Fig. 2B) occurs during this period. To resolve this discrepancy, we performed Strahler analysis[12] on anti-KRT19-stained bile ducts. Anti-KRT19 staining marks cholangiocytes only and is thus more suitable for the imaging of bile duct networks (rather than their luminal surfaces) (Fig. 3A). Strahler analysis is performed by skeletonization of the duct profile by pixel removal from all sides until only a single pixel trace of the duct is left (Fig. 3B).

Evaluation of the skeletons showed an increase in bi- and trifurcations of the biliary duct by day 3 followed by

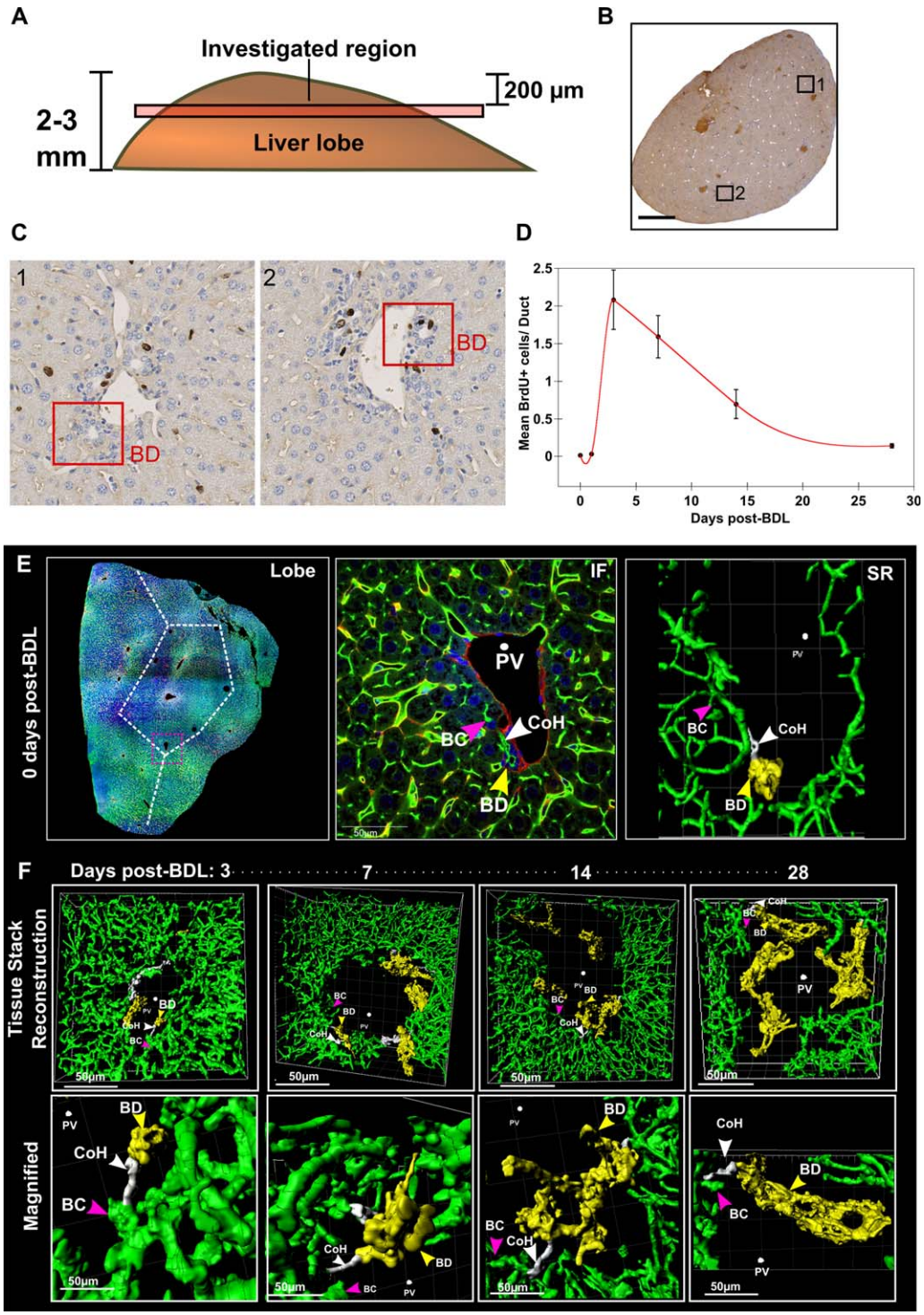

FIG. 1. (A) Location of vibratome tissue sectioning. The red bar indicates the region of the liver lobe that was investigated. (B) Representative anti-BrdU-stained lobular tissue section with peripheral portal fields indicated as insets 1 and 2. (C) Magnified view of portal fields in panel B with BrdU-positive cells (dark brown) and insets showing bile duct cross sections. (D) Quantification of proliferation indices (BrdU-positive cells) in bile ducts on various days post-BDL. Points indicate the mean ± standard error of the mean per time point, respectively. The trend line indicates the non-rounded Akima spline. (E) Left panel: Representative confocal micrograph tissue section with architectural staining (red, anti-mIgG [sinousoids]; green, anti-DPP4 [apical membranes including canaliculi]; gray, anti-GS [pericentral region]; blue, DAPI [cell nuclei]) showing a putative liver lobule (white dotted lines) based on portal field arrangement. The inset (pink dotted lines) indicates a single portal field. Center panel: Magnified view of the architectural immunofluorescence (IF) of the inset showing the portal vein (PV), bile canaliculi (BC), canals of Hering (CoH), and bile ducts (BD). Right panel: 3D surface reconstructions (SR) of the same features as in immunofluorescence from the corresponding confocal Z-stack. (F) Top row: Representative 3D surface reconstructions of confocal Z-stacks from various days post-BDL demonstrating the presence of bile ducts (BD, yellow), canals of Hering (CoH, white), and bile canaliculi (BC, green). Bottom row: Magnified view of the structures indicated in the top row. Scale bars: 50 μm.

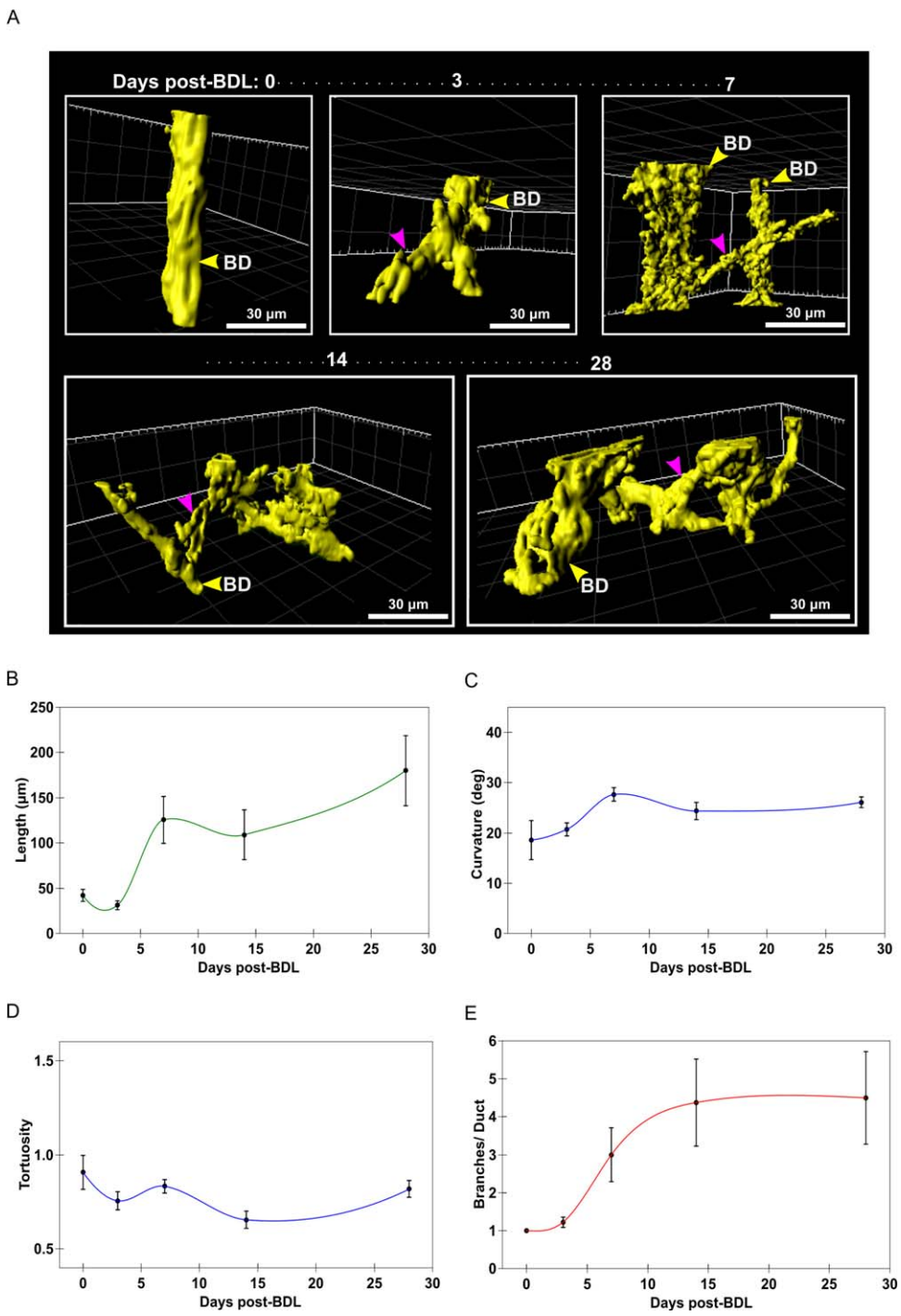

FIG. 2. (A) Representative bile ducts isolated from 3D surface reconstructions of the luminal surface from anti-DPP4 staining at various days post-BDL. Bile ducts parallel to the portal vein (yellow arrows) are shown with their interconnecting branches (magenta arrows). Scale bars: 30 μm. (B) Quantification of mean length of the bile ducts at various days post-BDL showing a biphasic increase. (C) Quantification of bile duct curvature along its axis at various days post-BDL. (D) Quantification of bile duct tortuosity at various days post-BDL. (E) Quantification of branches per bile duct at various days post-BDL showing logistic increase (Hill coefficient [p], 3.73; half-max [x_0], 6.73 days). Points indicate the mean ± standard error of the mean per time point, respectively. Trend lines indicate the non-rounded Akima spline for panels B-D. The line in panel E indicates regression fit of the data to $y = y_{min} + (y_{max} - y_{min})/[1 - (x - x_0)^p]$ with $R^2 = 0.99$.

a decrease at later time points (Fig. 3C). In addition, the average branch length increases steadily over 28 days post-BDL, thus accounting for the increase in overall duct length during this period (Fig. 3D). On the other hand, the overall complexity of the bile duct as measured by its ramification ratio (number of features per unit length of the duct) does not change significantly over the 28 days post-BDL (Fig. 3E). Indeed, on average, duct branches are typically of the first or second order, suggesting that most branches arise from the original unbifurcated duct or from first-order branches. Second-order branches rarely branch further. The complexity of

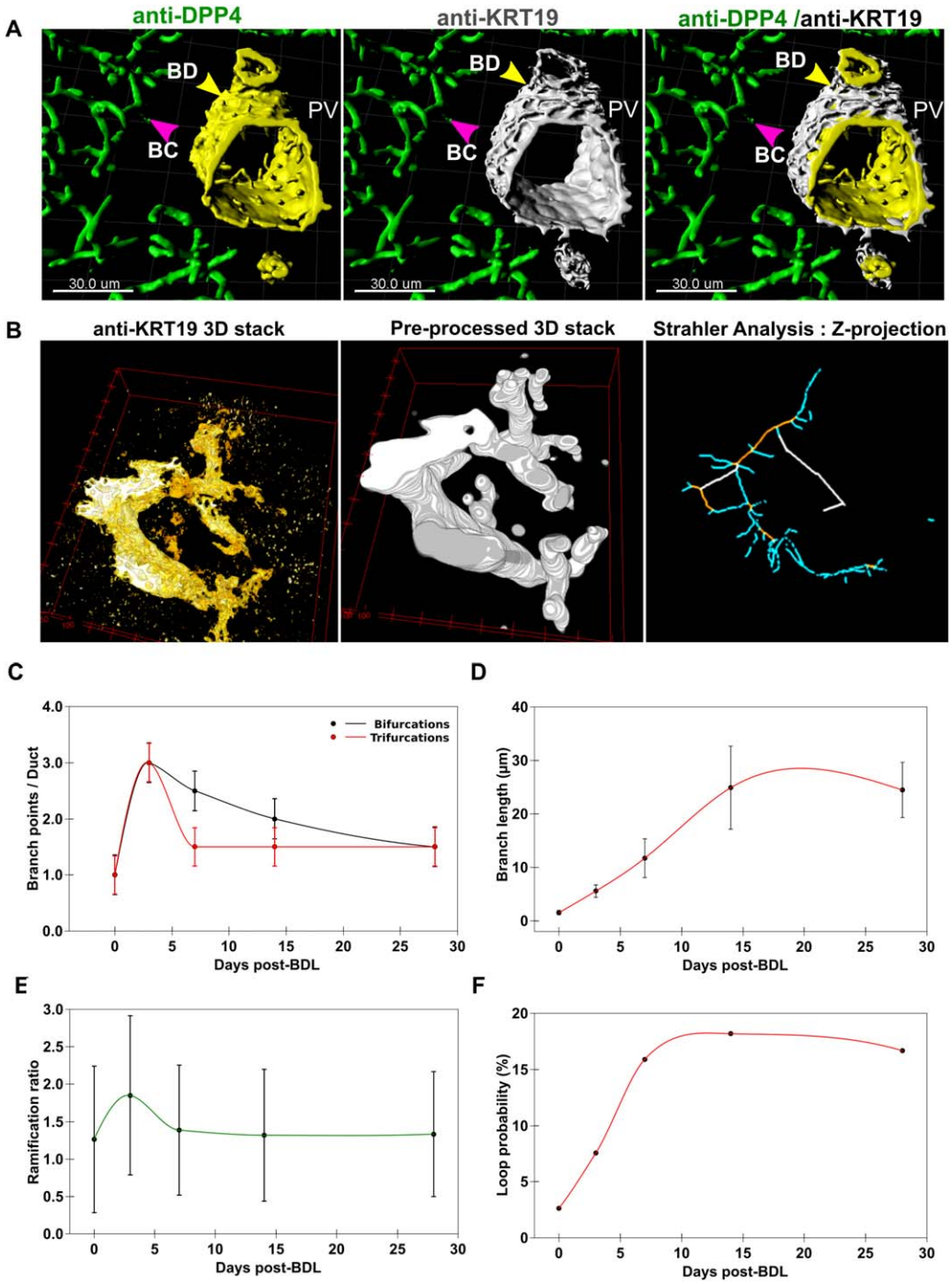

FIG. 3. (A) Representative surface reconstructions showing that DPP4 (left) and KRT19 (center) staining demarcate the bile duct equally well. DPP4 marks the luminal membrane surface, whereas KRT19 represents cytoskeletal secondary filaments of cholangiocytes as shown in the overlay (right). (B) Left: raw 3D-confocal data of a representative anti-KRT19 stained bile duct. Center: Gaussian-filtered volumetric representation of the bile duct (pre-processing). Right: Strahler analysis of the skeletonized processed image yields branch orders (color-coded), branch points, and branch lengths. (C) Frequency of branch points (bifurcations and trifurcations) per duct over various days post-BDL indicating that most branching occurs between days 3 and 14. (D) Quantification of branch length shows that branches elongate up to day 14. (E) Bile duct complexity is quantified as a ramification ratio that does not change significantly post-BDL. (F) Probability of loop formation (self-joining of branches). Points in all graphs indicate the mean ± standard error of the mean for bile ducts per time point in panels C-E. Points in panel F indicate ratio of loops to bile ducts per time point. Trend lines in all graphs indicate the nonrounded Akima spline.

the duct is defined by a ramification ratio, which indicates the number of orders of branches that occur in the duct per unit length of the duct. The constant ramification ratio is explained by the increasing probability of loop formation (Fig. 3F). Loop formation is defined as the rejoining of the branches to establishing a circular feature, which is excluded from the branch count. The probability of loop formation increases with the number and length of branches increase, reaching a maximum at day 14. Thus, it is apparent that branches tend to rejoin the existing ductular mesh, resulting in a constant overall duct complexity. The rejoining of the branches from day 3 onward may imply that alternative routes for bile flow are explored to circumvent potential blockages or dysfunctional duct segments. However, rejoining would also reduce the chances of finding an alternative pathway to eject bile if rejoining occurs to blocked or dysfunctional ducts. It is likely that rejoining of branches is a coincidental consequence of ductular elongation and branching within the constrained space between the portal vein and parenchyma. Nonetheless, the data presented here demonstrate that as a whole, the architecture of the interlobular biliary tree is significantly modified from a relatively sparse mesh that branches on average at every 100 μm to a complex mesh that branches every 20 μm. On the other hand, the degree of convolution of biliary ducts remains unaltered.

MECHANISTIC RESTRAINTS IN REMODELING OF THE BILIARY TREE

Because the bile duct is a transport structure for bile produced in the lobule, we investigated whether the increase in ductular tissue also leads to widening of the bile duct lumen. Increase in the cross-sectional diameter of common and interlobular bile ducts is considered a diagnostic indicator of injury[13] and obstruction[14] within the biliary tree. Furthermore, it has been suggested that BDL and cholestasis result in an increase in hydrostatic pressure due to the accumulation of excess biliary fluid in the biliary tree.[15] The excess pressure may be neutralized by an increase in the volume of the biliary tree. Although these studies were performed on large bile ducts that were clinically accessible, an increase in diameter throughout the biliary tree is a geometrically potent mechanism of increasing ductular volume, which varies with the square of the cross-sectional diameter. We therefore investigated whether BDL-induced cholestasis leads to an increase in the diameter of the interlobular bile ducts based on segmented intensity of anti-DPP4-stained bile ducts. Automated mean diameter, eccentricity, and area measurements were performed in cross-sectional planes perpendicular to the long axis to ensure that perspective and skewing effects do not lead to over- or underestimation of the duct diameter (Fig. 4A, Supporting Fig. S2B-D). The diameter of the duct remained invariant ($\sim$10 μm) over the 28-day examination period (Fig. 4B). This result was counterintuitive given the previous studies on larger bile ducts. We therefore further tested the possibility that changes in the cross-sectional eccentricity (deviation from a circular shape) may lead to an increase in the cross-sectional area of the duct and/or its branches without affecting the mean diameter. However, we found that while the average duct cross-section is eccentric (i.e., not a perfect circle), there are no significant changes in its eccentricity of the entire dataset comprising 39 ducts and their branches from three mice per time point over the 28 days post-BDL (Fig. 4C). We thus conclude that BDL-induced cholestasis does not lead to widening of the interlobular bile duct or its branches.

Because the diameter remains invariant over 28 days post-BDL, it is apparent that the substantial amount of cholangiocyte proliferation is directed toward the formation of ductular branches and their lengthening. It is possible that these branches are forced to extrude from the portal tract and invade the liver parenchyma. Chronic cholestasis eventually leads to fibrosis, which manifests itself as collagen-filled "fibrotic streaks" that invade the parenchyma and interconnect portal tracts.[16] Such ductular invasion of the liver parenchyma has been reported when hepatocyte regeneration is impaired following chemical injury, presumably "delivering" hepatic progenitors to the parenchyma through small penetrating bile ducts.[3,4,17] We therefore investigated whether the excess ductular tissue penetrates the liver parenchyma by measuring the pixel-wise distance between bile ducts and the portal vein. Contrary to the specific scenarios with 3,5-diethoxycarbonyl-1,4-dihydrocollidine (DDC), choline-deficient ethionine-supplemented (CDE), or CCl_4 studied thus far,[3] we observed instead that bile ducts maintain a constant distance from the wall of the portal vein throughout the 28 days post-BDL (Fig. 4D). Isolated KRT19-positive cells[18] do occur as in control (Fig. S2C), but in particular, we do not see any branches or ductules that invade the parenchyma of the liver. There is little to no change in the diameter of the portal vein, nor in the diameter of the bile duct. Thus, the bile duct apparently lengthens and branches, but all ductular tissue remains constrained to within 10

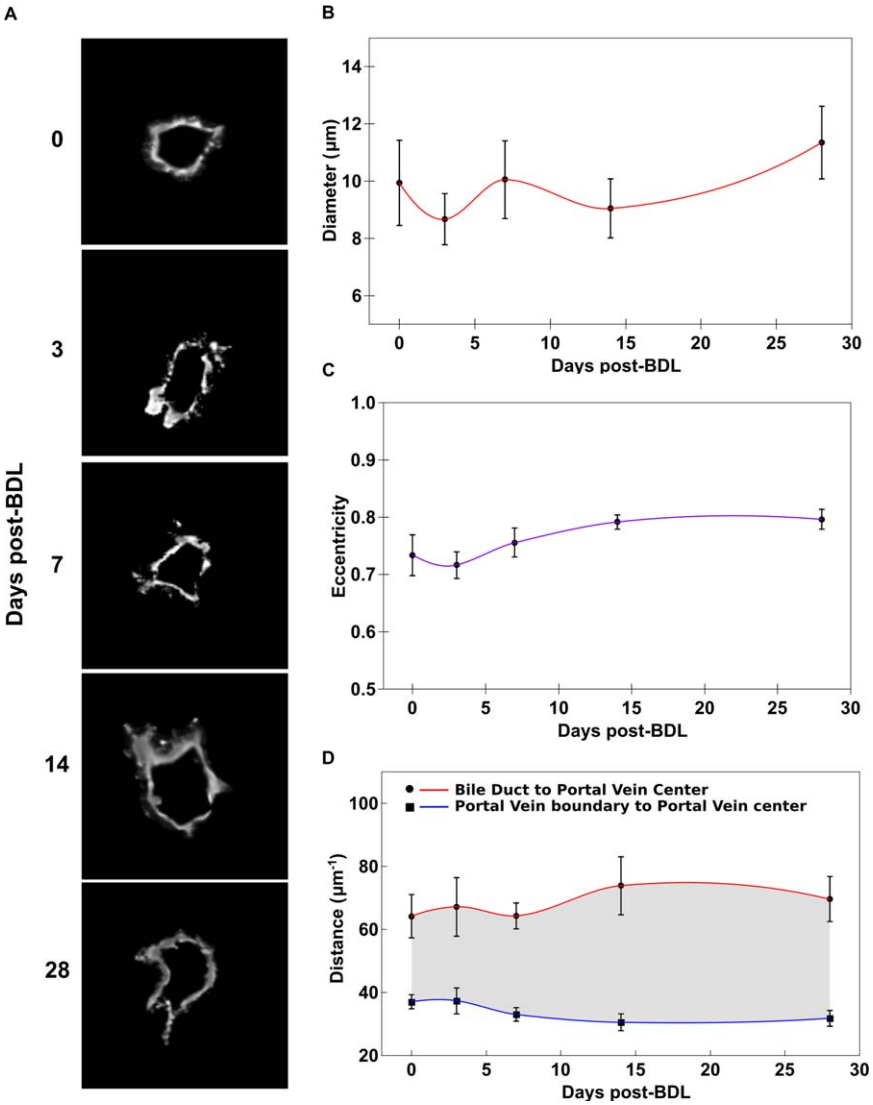

FIG. 4. (A) Representative segmented cross-sections of bile ducts from various days post-BDL. Scale bar: 10 μ m. (B) Quantification of bile duct diameter showing no significant change at various days post-BDL. (C) Quantification of bile duct eccentricity showing no significant change at various days post-BDL. (D) The difference (gray area) between the radius (blue) of the portal vein and the distance of bile ducts (red) from the portal vein center indicates that bile ducts maintain a constant distance from the portal vein wall at various days post-BDL. Points in all graphs indicate the mean ± standard error of the mean for bile ducts per time point. Trend lines in all graphs indicate the non-rounded Akima spline.

to 15 μm of the portal vein. Together, these data show that ductular reactions are governed by tissue modeling principles; lengthening and branching occurs with specific restraints on the diameters of the bile ducts/branches as well as maintaining their proximity to the portal vein.

ENLARGEMENT OF THE BILIARY TREE DESPITE RESTRAINTS

In the context of volumetric increase of the biliary tree to accommodate excess bile, we next investigated the effects of increasing length and branching with an unchanging diameter on ductular volume. The length and diameter measurements allowed us to calculate the expected ideal volume of the observed biliary duct as $\pi r^2 L$, assuming that the duct is perfectly cylindrical. We compared the cylindrical volume with the volume measured from 3D intensities (Fig. 5A) of the bile duct as an integration of the cross-sectional areas determined earlier. Voxel-based quantification of the ductular luminal volume demonstrated an approximately five-fold increase until day 28 compared with controls. This increase was not monotonic, but rather occurred in two distinct phases between days 3 and 7 and between days 14 and 28, respectively. The absolute values and changes in the measured volume of the duct followed the ideal cylindrical volume closely. The constant positive offset in the measured volume is likely the effect of the constant but nonzero eccentricity and tortuosity of the

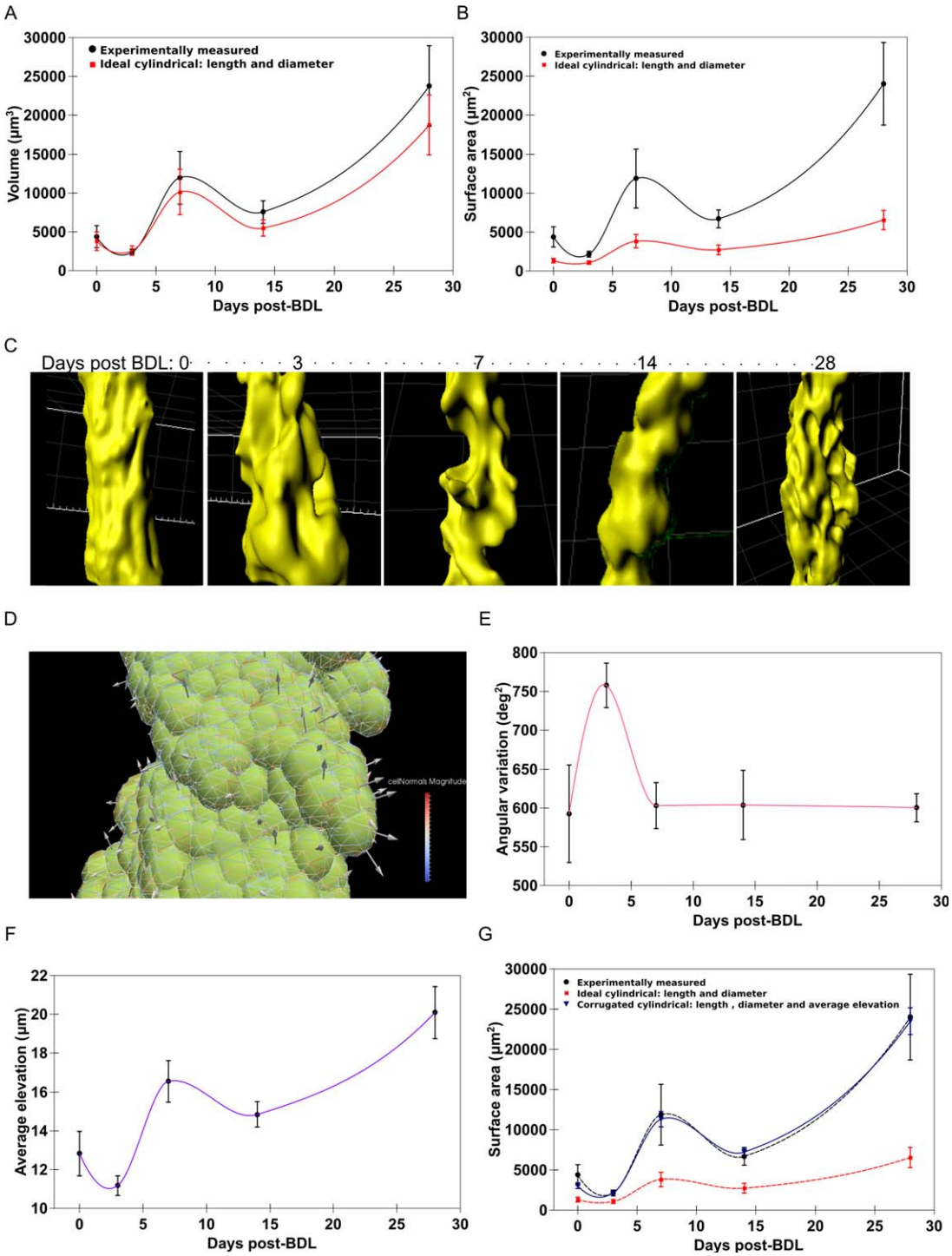

FIG. 5. (A) Experimentally determined (black) and ideal cylindrical (red) bile duct volume showing a biphasic increase from days 3 to 7 and days 7 to 28 post-BDL. Experimentally determined volume is derived from summation of voxels representing the bile duct in 3D confocal Z-stacks. The ideal cylindrical volume is calculated as ($\pi r^2 L$) from length and diameter measurements of these bile ducts. Close approximation between these parameters indicates that increase in volume is driven by increase in duct length post-BDL, as the diameter remains invariant. (B) Experimentally determined (black) and ideal cylindrical (red) bile duct surface area showing biphasic increase from days 3 to 7 and days 7 to 28 post-BDL. Experimentally determined surface area is derived from summation of triangle areas constituting bile duct surfaces in reconstructed 3D confocal Z-stacks. The ideal cylindrical surface is calculated as ($2\ \pi rL$) from length and diameter measurements of these bile ducts. (C) Representative bile duct surfaces generated from anti-DPP4 staining at various days post-BDL showing the presence of corrugations on the luminal duct surface. (D) Representative bile duct with automated tessellation and normals computation (arrows) to quantify surface corrugation. (E) Quantification of angular variance between normal vectors at various days post-BDL. (F) Quantification of corrugation amplitude (average elevation of surface) from normal vector magnitudes at various days post-BDL. (G) Experimentally determined (black) and ideal cylindrical (red) bile duct surface area as in panel A, along with corrugated cylindrical surface area (blue) calculated from the average elevation in panel E. Close approximation between experimentally determined and corrugated cylindrical surface area indicates that the increase in surface area occurs due to increase in corrugation amplitude. Points in all graphs indicate the mean ± standard error of the mean of bile ducts per time point, respectively. Trend lines in all graphs indicate the nonrounded Akima spline.

ducts, reflecting the fact that the duct is not a geometrically perfect cylinder. Bile duct volume varies linearly with length, and closely approximates the volume-length relationship of a perfect cylinder. It is clear that the changes in volume are predominantly explained by the elongation of the duct.

EXPANDED DUCT LUMINAL SURFACE THOUGH CORRUGATION

Ductular reactions do not seem to be geometrically optimized to increase ductular volume; rather, the volume increases suboptimally due to increase in length. In retrospect, this is not surprising, as a major function of cholangiocytes is the modification of biliary fluid by reabsorption or secretion of bile salts, water, and electrolytes.[1,19] Transporters and enzymes that are involved in this modification are present on the apical membrane of cholangiocytes (i.e., on the luminal surface of the bile duct). An increase in ductular tissue also increases the functional capacity of the biliary tree to reabsorb bile salts and thereby alleviate cholestasis through the cholehepatic shunt.[2,19,20] We therefore investigated whether cholangiocyte proliferation leads to an enhancement of luminal surface area of the bile duct, thereby enlarging the interface between the cholangiocyte apical membrane and ductular bile.

To accurately measure the surface area, we generated isosurface tessellations of the DPP4 stained luminal membrane of segmented bile ducts. At 28 days post-BDL, a dramatic five-fold increase in the surface area was observed (Fig. 5B). Moreover, the measured surface area of the bile duct was also approximately four-fold higher than the ideal cylindrical surface area calculated from length and diameter measurements as $2\pi rL$. The large discrepancy between these values shows that an increase in bile duct surface area cannot be explained merely by an increase in bile duct length. Close examination of the generated bile duct surfaces showed the presence of corrugations on the luminal bile duct surface (Fig. 5C). Indeed, examples of reconstructed surfaces showed a relatively smooth luminal bile duct surface in control mice but a much more uneven, wrinkled surface after BDL. We hypothesize that these corrugations may explain the observed disproportionate increase in surface area, analogous to the function of villi in the intestine or sulci in the brain, where an expansion of absorptive and cortical surface area, respectively, is achieved within a restricted volume through ex- or invagination of a 2D planar tissue surface into 3D.

To quantify the extent of corrugation, we used duct surface isosurfaces to determine the average elevation (amplitude) and angular variation (frequency) over the 28-day observation period post-BDL. Isosurfaces were generated for the surface area quantification, which comprised individual triangles for which orientation vectors and normals were calculated (Fig. 5D). The magnitude of the normals indicates the extent of displacement from an ideal planar surface at that point which is the average elevation. The direction of the normals indicates the angle of the displacement and reflects the frequency of corrugations. Together, the average elevation and angular variance form a measure of corrugation (or roughness). In the 28 days after BDL, the variance in the roughness peaked at day 3 and returned to control levels until the end of the observation period (Fig. 5E). However, the corrugation amplitude (average elevation) increased in two steps between 3 and 7 as well as 14 and 28 days, similar to the biphasic increases observed for length, volume and surface area (Fig. 5F).

To test whether the degree of increase in the ductular length and the degree of corrugation quantitatively explain the increased surface area, we simulated surfaces of varying length and roughness (Supporting Information, "Simulation of Corrugated Surfaces"). The simulation shows that the surface area varies with direct proportion to the average elevation of the corrugations, and periodically with the angular variation of the corrugations (Fig. S3). Using the empirically measured values, we then calculated surface area as a function of length, diameter, angular variation and average elevation over the 28 days post-BDL. This calculated surface area results in a near perfect match with the measured surface area at these time points (Fig. 5G), thereby eliminating the apparent discrepancy between measured and smooth cylindrical surface areas shown earlier.

REDUCTION OF DUCT-CANALICULAR CONNECTIVITY

During BDL-mediated cholestasis, bile acid metabolism is significantly altered in hepatocytes and cholangiocytes.[15,21,22] These changes, however, do not necessarily affect the amount of biliary fluid generated in the bile canalicular network,[23,24] but rather only the bile salt concentrations. We investigated whether the increase in the overall length of bile ducts and the number of branches post-BDL also lead to enhanced connectivity of the lobular canalicular network. To that extent, we measured the frequency of canals of Hering

on interlobular bile ducts. Canals of Hering represent connections of the canalicular network to bile ducts (Fig. 6A, top) and thereby directly reflect the capacity of the bile duct to drain hepatocyte-generated biliary fluid. The frequency of Hering canals per unit length of bile duct decreased over the 28-day post-BDL period from ~5 in every 100 μm of duct to ~1 in every 100 μm of duct (Fig. 6A, bottom, red line). To rule out the possibility that this decrease merely reflects the effect of bile duct elongation, we also measured the frequency of Hering canals per unit length of the portal vein. The frequency of Hering canals remained at a constant value of 1 to 2 for every 100 μm of portal vein until day 7, with a decrease at 14 and 28 days post-BDL. This result shows that although the ducts elongated, no new Hering canals were established. Instead, the relative capacity to drain bile from the canalicular network into the interlobular bile ducts was reduced, suggesting a response to curtail elevated bile salt concentrations present in the duct during cholestasis.

Discussion

The results of this study demonstrate a complex spatio-temporal response of the biliary tree in response to cholestatic stress induced by BDL. The correlation map in Fig. 6B depicts the interdependency of various morphometric and experimental parameters and their changes over time after BDL. The comprehensive quantification of duct morphology and cellular proliferation allowed us to piece together the major phases of this tissue-level adaptive response (Fig. 7). In all cases, morphological changes of the duct occurred in two phases, which are distinguished as an acute and chronic phase based on serum markers and cellular proliferation rate. In brief, the timeline of architectural changes following BDL is as follows. Before exposure to any cholestatic stress, interlobular bile ducts exist as a sparse mesh with <0.5% cholangiocyte proliferation rate. Exposure to cholestatic stress for 3 days results in a strong proliferative response of cholangiocytes reflected in the pronounced corrugation of the luminal surface of the bile duct. Corrugation results in a concomitant increase of the ductular luminal surface area. At day 3 after ligation, bile ducts also present a novel feature, the occurrence of bifurcations and trifurcations indicating the start of ductular branching. Branching proceeds in a cooperative manner until day 14. Upon continued cholestasis until day 7, the proliferation rate diminishes but still remains above control levels. For the first time since BDL, an increase in duct length is

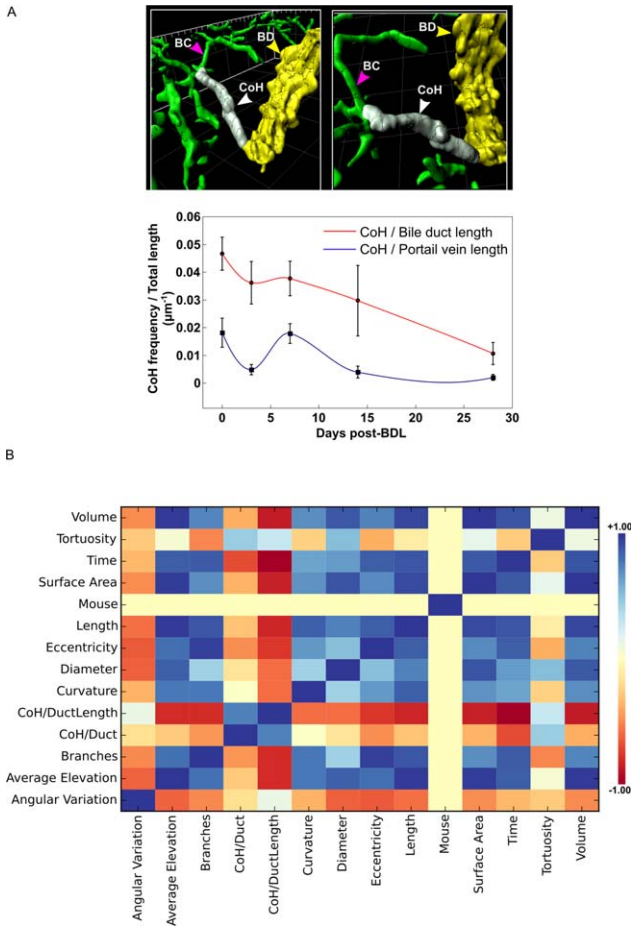

FIG. 6. (A) Top panel: Two views of a representative 3D surface reconstruction of an isolated canal of Hering (CoH) showing the connection between a bile duct (BD) and bile canaliculi (BC). Bottom panel: Occurrence of canals of Hering per unit length of bile duct (red) and per unit length of the portal vein (blue) at various days post-BDL showing a decrease of canals of Hering density post-BDL. Points in all graphs indicate the mean ± standard error of the mean per time point. Trend lines in all graphs indicate the nonrounded Akima spline. (B) Heat map showing correlation of all measured parameters. Salient features include (1) strong (>0.90) positive correlation between average elevation of corrugations, length, surface area, time, and volume; (2) strong (< −0.9) negative correlation between canals of Hering per unit bile duct length and time; and (3) weak or no (−0.5 < 0 < 0.5) correlations between all other parameters.

observed. This is accompanied by a reduction in the frequency of corrugation but with simultaneous increase in their amplitude of the remaining corrugations. Therefore, the length increase may be explained as a relaxation process. This indicates that the transient increase in corrugation frequency acts as a temporal buffer, which introduces the delay between duct elongation and maximal duct proliferation rate. At day 7,

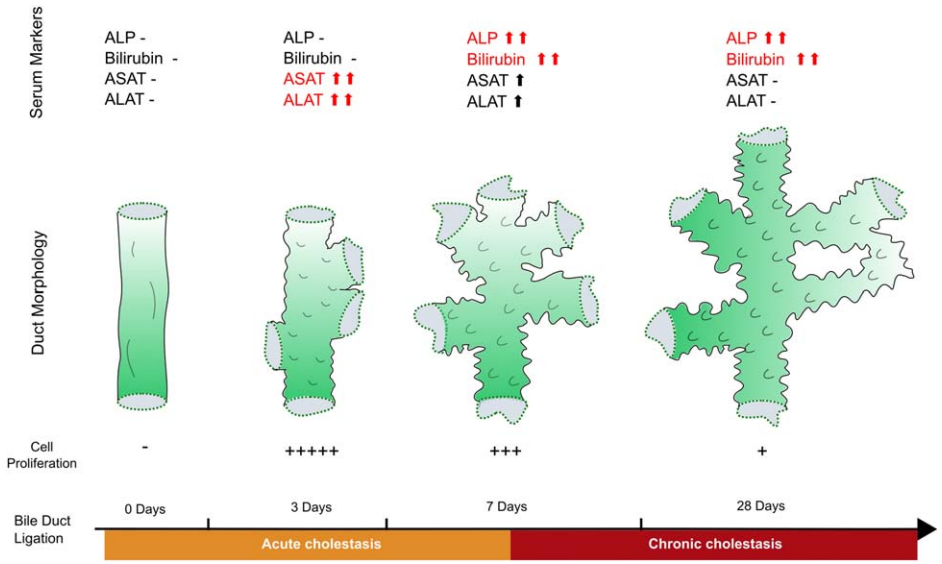

FIG. 7. Ductular reaction after BDL. Changes in serum chemistry, bile duct morphology, and cell proliferation at various days following BDL. Biphasic trends in bile duct reactions, differences in specific early and late serum markers of liver injury and differences in cellular proliferation rate show the existence of distinct temporal phases in cholestatic injury. Acute cholestasis is associated with high cellular proliferation, acute liver injury, the first phase of duct elongation, branching, the appearance and increase of luminal surface corrugation and corresponding increase in ductular surface area and volume. Chronic cholestasis represents the second phase where duct elongation continues, branching is superseded by self-joining of the branches to form loops, corrugation increases in amplitude but not frequency and relative density of duct-to-canalicular network connections is reduced. Elevation of serum markers of acute liver injury is supplanted by serum markers of jaundice.

the duct length increases but is accompanied by a reduction in the number of bifurcations, and no change in the average branch length. From day 7 to day 14, the probability of loop formation increases to a maximum, and negates the cooperative effect of branch formation. Thus loop formation restricts the extent of branching to the formation of second order branches. The frequency of the canals of Hering (connections of the duct to the canalicular network) decreases moderately from ~1 every 20 μm to 1 every 25 μm of bile duct. These changes mark the end of the acute phase ductular response. The chronic phase from day 14 to day 28 is characterized by a reduction in cellular proliferation and a further increase in ductular length, volume, and surface area. On the other hand, branching frequency and probability of loop formation are maintained at their maximal levels reached on day 14. In this chronic cholestatic phase, the frequency of canals of Hering reduces precipitously ~1 every 100 μm of bile duct as a result of duct elongation. Duct diameter, eccentricity, curvature, and tortuosity remain invariant over the 28-day post-BDL period. The bile duct itself and its branches remain confined to within 10 to 15 μm of the portal vein over the entire period.

In the context of ductular diameter, the present findings show that the mean bile duct diameter remains invariant over 28 days after BDL. This discrepancy with previous reports may be explained by the distinct regions of the biliary tree that were analyzed. Surgical or radiological approaches are limited to the common or extrahepatic bile duct or to the large intrahepatic bile ducts. Radiological approaches such as micro-CT are limited by their resolution to structures larger than 30μm. Traditionally, structures smaller than 30μm have been analyzed in 2D sections, examining only a projection of the 3D architecture of the lobule and thereby losing information about processes such as surface wrinkling and branching properties. Furthermore, 2D sectioning introduces bias, because the more complex a 3D biliary mesh becomes, the less likely it is to find a single sectioning plane that is perpendicular to the long axis of all branches. We illustrate this bias by using our 3D duct reconstructions to show the discrepancy in diameter measurements made with and without prior knowledge of the long axis of the duct (Fig. S2D). Consistent with this, we would have observed significantly higher duct diameters from day 7 to day 28 post-BDL in 2D sections of our data.

Using full 3D geometry and determining the long axis of the ducts prior to diameter measurement mitigates this bias. Therefore, it should be considered that analyzing ductular reactions in 2D will inevitably lead to overestimation of duct diameter with increasing branching frequency.

Morphometry of the terminal branches of the biliary tree that penetrate the functional unit of the liver—namely, the hepatic lobules—is only accessible through 3D confocal microscopy. The response of these interlobular ducts has not been documented thus far. The present study provides the first description of the response of structures ranging from 0.207 to 30 μm in 3D, thereby illuminating the blind spot between the large bile ducts and bile canaliculi. Whereas previous studies focusing on large ($\sim$200 μm) bile ducts have reported the major alteration to be an increase in duct diameter,[13] events in the range of smaller bile ducts are much more complex.

The adaptive tissue response described herein seems finely tuned to optimize the interface of the duct lumen to the cholangiocyte apical membrane. The parameter showing the maximal increase is the luminal surface area, which is achieved through lengthening and the hitherto unknown component of corrugation. In contrast, the parameter that would maximize the duct volume—the ductular diameter—remains unchanged. The cholangiocyte apical membrane contains a plethora of bile salt transporters, aquaporins, and ion channels that modulate bile composition. BDL-induced cholestasis can only be resolved by reabsorption of bile constituents via the cholangiocytes.[1,5,25] Adaptive responses at the cellular level, such as up-regulation and recruitment of bile transporters to their apical membrane in response to cholestasis, have been demonstrated previously.[19] The present study describes a tissue-level adaptive response that augments the cellular response by enhancing the surface area available for the resorption of bile salts. This interlobular duct tissue response can be contrasted with the response of larger bile ducts, wherein the volume is maximized. Volume expansion optimizes both fluid flow (advection) and rather minimizes the surface area. In principle, both the large and small (terminal) bile ducts could increase their diameter to gain larger luminal volume. However, it is likely that the small terminal bile ducts have higher resorption capacity than the large bile ducts. This is consistent with their adaptive response to maximize their surface area. In contrast, cholangiocytes of the large bile duct may have limited absorption capacity for bile salts and serve more as water conduits.[26] In case of pathological bile duct obstructions, an increase in the diameter of large bile ducts will undoubtedly increase the chances that flow in large bile ducts will be restored if the luminal diameter of the ducts becomes larger than the size of the obstruction. Indeed, a terminal bile duct will receive bile from only one or a limited number of lobules. On the other hand, the number of lobules that eventually drain into a large bile duct increases the closer the duct segment is to the root of the biliary tree (i.e., the common bile duct). Thus, the volume problem is much more severe closer to the site of the ligation in the common bile duct. The capacity of the interlobular bile duct to receive bile diminishes as no new canals of Hering are formed, despite the increase in the overall size of the interlobular biliary tree. Still, they must accommodate the normal amount of generated bile into their lumen, even if there is no increase in biliary efflux from the lobule. It is possible that resorption of bile by cholangiocytes may serve to alleviate this problem somewhat; under chronic conditions, however, this resorptive capacity of cholangiocytes is likely overwhelmed. The present tissue-level reconstructions thus demonstrate the distinct adaptive principles of the interlobular versus higher-order (i.e., larger) bile ducts.

In a recent study, a similar 3D morphometric approach has been used efficiently to understand the morphogenesis of bile ducts during embryonic development.[8] The authors report that duct formation occurs through initial formation of precursor cell clusters, which next elongate to form segments and finally fuse to generate a *de novo* bile duct including all its branches. Similarly, dispersed solitary KRT19-positive cells have been reported to contribute to adult ductular reactions induced by 3,5-diethoxycarbonyl-1,4-dihydrocollidine (DDC) treatment or choline-deficient ethionine-supplemented (CDE) diet by forming small ductules.[18] However, it is clear that these processes are completely distinct from the response of adult bile ducts to cholestasis. Following BDL, adult bile duct cells remain differentiated, and branches can only arise from preexisting ducts. Although we also observed solitary KRT19-positive cells (Supporting Fig. S2C), we never observed fragmented ductules that may have arisen from these cells. Neither is *de novo* cholangiogenesis of the kind seen in embryonic development observed following BDL. In a second 3D confocal study the architecture of the biliary ducts in the mouse liver was analyzed after administration of hepatotoxic chemicals.[3] The authors observed that the

hepatobiliary system remodels, whereby the biliary branches extend to the pericentral necrotic area after chronic CCl_4 or thioacetamide exposure in mice. Such a pericentral bile duct infiltration was also not observed in the present study. In contrast, the mesh of bile ducts remained always in close proximity to the portal veins. However, it should be considered that the present study reconstructed the bile duct system after ligation of the common bile duct, which in contrast to CCl_4 does not lead to pericentral necrosis.

In conclusion, the present study demonstrates how an initially sparse ductular network elongates, corrugates, and ramifies during cholestasis. These responses may be specific for the interlobular ducts, and are qualitatively different from those observed in larger bile ducts as well as mechanistically distinct from bile duct development during embryogenesis. The results underscore the significance of architectural interlobular bile duct adaptive responses in enhancing cellular functions that alleviate cholestasis.

Acknowledgment: We thank Isabelle Leclercq, Neil Theise, and Laurent Dollé for valuable commentary and stimulating discussion. We also thank Brigitte Begher-Tibbe for technical support.

REFERENCES

1) Strazzabosco M. Transport systems in cholangiocytes: their role in bile formation and cholestasis. Yale J Biol Med 1997;70:427-434.
2) Alpini G, Ulrich C, Roberts S, Phillips JO, Ueno Y, Podila PV, et al. Molecular and functional heterogeneity of cholangiocytes from rat liver after bile duct ligation. Am J Physiol 1997;272: G289-G297.
3) Kaneko K, Kamimoto K, Miyajima A, Itoh T. Adaptive remodeling of the biliary architecture underlies liver homeostasis. HEPATOLOGY 2015;61:2056-2066.
4) Gouw ASH, Clouston AD, Theise ND. Ductular reactions in human liver: diversity at the interface. HEPATOLOGY 2011;54:1853-1863.
5) Roskams T, Desmet V. Ductular reaction and its diagnostic significance. Semin Diagn Pathol 1998;15:259-269.
6) Tag CG, Sauer-Lehnen S, Weiskirchen S, Borkham-Kamphorst E, Tolba RH, Tacke F, et al. Bile duct ligation in mice: induction of inflammatory liver injury and fibrosis by obstructive cholestasis. J Vis Exp 2015:52438.
7) Lee BS, Kim NJ, Jeong HY, Lee HY, Kang DY, Noh SM. Changes in serum cytokine concentration: a morphological study of liver cirrhosis induced by common bile duct ligation in rats. Korean J Intern Med 2003;18:6-12.
8) Takashima Y, Terada M, Kawabata M, Suzuki A. Dynamic three-dimensional morphogenesis of intrahepatic bile ducts in mouse liver development. HEPATOLOGY 2015;61:1003-1011.
9) Masyuk T V, Ritman EL, LaRusso NF. Quantitative assessment of the rat intrahepatic biliary system by three-dimensional reconstruction. Am J Pathol 2001;158:2079-2088.
10) Hammad S, Hoehme S, Friebel A, von Recklinghausen I, Othman A, Begher-Tibbe B, et al. Protocols for staining of bile canalicular and sinusoidal networks of human, mouse and pig livers, three-dimensional reconstruction and quantification of tissue microarchitecture by image processing and analysis. Arch Toxicol 2014;88:1161-1183.
11) Prinz H. Hill coefficients, dose-response curves and allosteric mechanisms. J Chem Biol 2010;3:37-44.
12) Schwen LO, Preusser T. Analysis and algorithmic generation of hepatic vascular systems. Int J Hepatol 2012;2012:357687.
13) Senturk S, Miroglu TC, Bilici A, Gumus H, Tekin RC, Ekici F, et al. Diameters of the common bile duct in adults and postcholecystectomy patients: a study with 64-slice CT. Eur J Radiol 2012;81:39-42.
14) Parulekar SG. Ultrasound evaluation of common bile duct size. Radiology 1979;133:703-707.
15) Georgiev P, Jochum W, Heinrich S, Jang JH, Nocito A, Dahm F, et al. Characterization of time-related changes after experimental bile duct ligation. Br J Surg 2008;95:646-656.
16) Tannuri ACA, Coelho MCM, de Oliveira Gonçalves J, Santos MM, Ferraz da Silva LF, Bendit I, et al. Effects of selective bile duct ligation on liver parenchyma in young animals: histologic and molecular evaluations. J Pediatr Surg 2012;47:513-522.
17) Alison MR, Golding M, Sarraf CE. Liver stem cells: when the going gets tough they get going. Int J Exp Pathol 1997;78:365-381.
18) Jörs S, Jeliazkova P, Ringelhan M, Thalhammer J, Dürl S, Ferrer J, et al. Lineage fate of ductular reactions in liver injury and carcinogenesis. J Clin Invest 2015;125:2445-2457.
19) Xia X, Francis H, Glaser S, Alpini G, LeSage G. Bile acid interactions with cholangiocytes. World J. Gastroenterol 2006;12: 3553-3563.
20) Alpini G, Glaser SS, Ueno Y, Pham L, Podila P V, Caligiuri A, et al. Heterogeneity of the proliferative capacity of rat cholangiocytes after bile duct ligation. Am J Physiol 1998;274:G767-G775.
21) Fickert P, Zollner G, Fuchsbichler A, Stumptner C, Weiglein AH, Lammert F, et al. Ursodeoxycholic acid aggravates bile infarcts in bile duct-ligated and Mdr2 knockout mice via disruption of cholangioles. Gastroenterology 2002;123:1238-1251.
22) Heinrich S, Georgiev P, Weber A, Vergopoulos A, Graf R, Clavien P-A. Partial bile duct ligation in mice: a novel model of acute cholestasis. Surgery 2011;149:445-451.
23) Gleeson D, Murphy GM, Dowling RH. Effect of acute bile acid pool depletion on total and ionized calcium concentrations in human bile. Eur J Clin Invest 1995;25:225-234.
24) Lenzen R, Elster J, Behrend C, Hampel KE, Bechstein WO, Neuhaus P. Bile acid-independent bile flow is differently regulated by glucagon and secretin in humans after orthotopic liver transplantation. HEPATOLOGY 1997;26:1272-1281.
25) Kountouras J, Billing BH, Scheuer PJ. Prolonged bile duct obstruction: a new experimental model for cirrhosis in the rat. Br J Exp Pathol 1984;65:305-311.
26) Glaser SS, Gaudio E, Rao A, Pierce LM, Onori P, Franchitto A, et al. Morphological and functional heterogeneity of the mouse intrahepatic biliary epithelium. Lab Investig 2009;89:456-469.

Supporting Information

Additional Supporting Information may be found at onlinelibrary.wiley.com/doi/10.1002/hep.28373/suppinfo.